JOURNAL OF MATERIALS SCIENCE 37 (2002) 4481–4486

Solidification behaviors of the emulsified Al-4wt%Fe alloy powders

H. S. SEO, W. Y. YOON
Division of Materials Science and Engineering, Korea University, 1, 5 Ga, Anam-dong, Sungbuk-ku, Seoul, 136-701, Korea
E-mail: alloysam@korea.ac.kr

M. H. KIM
School of Materials Science and Engineering, Inha University, 253 Yonghyun-dong, Nam-gu, Inchon, 402-751, Korea

E. P. YOON
Division of Materials Science and Engineering, Hanyang University, 17 Haengdang-dong, Seongdong-Gu, Seoul, 133-791, Korea

K. H. KIM
Department of Mechanical Engineering, Korea University, 1, 5 Ga, Anam-dong, Sungbuk-ku, Seoul, 136-701, Korea

The emulsified Al-4wt%Fe alloy powders showed several different microstructures depending on the amount of undercooling such as $Al_{13}Fe_4$, Al_xFe primary intermetallic, Al-Al_3Fe or Al-Al_6Fe eutectics and α-Al cellular structure. The presence of these phases depends on a competitive growth mechanism, which was determined by the undercooling prior to solidification. The amount of undercooling of the powders was monitored by differential thermal analysis and was matched with the microstructures. The difference of the amount of undercooling which corresponds to the microstructures between the experiment and the previous value converted by the LKT theory was rationalized through the solidification behaviors. A microstructure selection map of Al-4Fe alloy powders for tailored solidification was also suggested. © *2002 Kluwer Academic Publishers*

1. Introduction

Al-Fe is an attractive system due to the fact that its microstructure can be altered by rapid solidification processing (RSP) [1] and that it is possible for better high temperature properties than conventional Al alloys [2].

A wide range of microstructures has been observed in Al-Fe alloys produced by splat-quenching [3], melt-spinning [4], atomization [5] and mechanical alloying [6]. The variability of microstructures suggests that melt undercooling prior to nucleation play an important role in phase selection [2].

Aluminum forms an eutectic with the stable intermetallic phase, Al_3Fe, as well as with the metastable phase, Al_6Fe. Other metastable binary phases have been observed as interdendritic precipitates: Al_xFe ($x = 5.0$–5.8) [7–9], Al_9Fe_2 [10, 11] and Al_mFe ($m = 4.0$–4.4) [12]. The observed solidification microstructures result from the competition in nucleation and growth of these phases in an Al-matrix of eutectic or dendritic morphology [13].

In this research, Al-4wt%Fe alloy powders were manufactured by the droplet emulsion technique (DET). The solidification temperature was measured quantitatively by differential thermal analysis (DTA) and the corresponding microstructures of emulsified Al-4Fe powders were examined. Therefore, using the undercooling and microstructures relationships, a microstructure selection map (MSM) for the system was built for materializing the "tailored solidification".

2. Experimental

The alloy was prepared using pure Al (shot-type, 99.9%) and Fe (wire-type, 99.9%) by induction melting under an argon gas environment. The measured chemical composition of Al was 96.12 wt% and Fe was 3.88 wt%.

Al-4wt%Fe (designated Al-4Fe) alloy powders were made in the LiCl-41.5mol%KCl molten salt by the droplet emulsion technique (DET). DET involves the emulsification of a mixture of liquid metal and a carrier fluid with a high-speed shearing device under an inert gas environment. By dispersing a liquid metal into fine particles, these nucleation catalysts are trapped within a small fraction of the particles. The majorities are free from impurities and can be highly undercooled [14]. The experimental apparatus are shown in Fig. 1. A mixture of the Al-4Fe alloy and the LiCl-KCl molten salt was sheared at 10,000–30,000 rpm to produce an emulsion. The final droplet size was in the range of 30–250 μm.

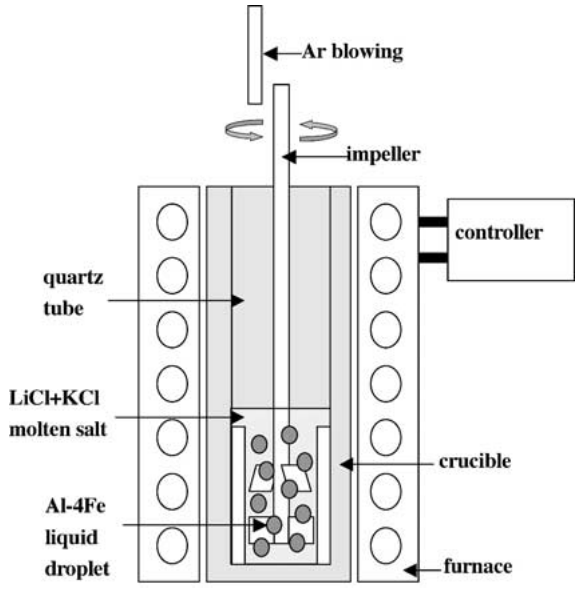

Figure 1 The diagram of an emulsification apparatus.

The melting and crystallization behaviors of powders were monitored by a differential thermal analysis (DTA, DT-7000 Sinku-Riko) at heating and cooling rates of 20 K/min.

The Al-4Fe powders were collected, rinsed and mounted for optical microscope (OPTIPHOT-100 Nikon) and scanning electron microscope (JSM-5310LV JEOL) examination. Keller's reagent (1% $HF + 1.5\%$ $HCl + 2.5\%$ $HNO_3 + 95\%$ H_2O) and 5% NaOH solution were used as etchants for optical images. The phases that were present in the powders were identified by X-ray microanalysis (EDS). An image Analyzer (BMI PLUS ver 2.19 BUMMI UNIVERSE) was used to examine the average size of the powders.

3. Results

Droplets of Al-4Fe were produced ranging in diameter from $\sim$30 μm to $\sim$250 μm. The size distribution and average size of Al-4Fe alloy powders were measured by an Image Analyzer as shown in Fig. 2. The average size of the droplets decreased with the rotating speed.

The undercooling response of Al-4Fe powders was studied with DTA. Undercooling attained depended, to a significant extent, on powder size. Fig. 3 shows DTA thermograms for various sizes. The heating curve shows two different endothermic peaks. The first peak, about

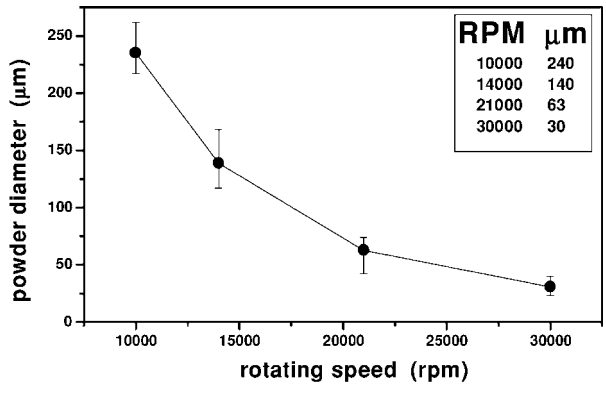

Figure 2 The experimental powder size distribution at given rotating speed.

TABLE I DTA results of Al-4Fe droplets

Powder size μm	Eutectic temp (°C)	Liquidus temp (°C)	T_N(onset) °C	T_N(peak) °C	ΔT (K)	$\Delta T/T_L$
240	646	750	718	713	37	0.03
140	650	750	671	665	85	0.08
63	648	756	622	616	140	0.13
30	656	751	599	591	160	0.16

TABLE II Summary of the EDS result of the primary $Al_{13}Fe_4$ and Al_xFe phase

Primary phase	wt%Fe	
$Al_{13}Fe_4$	35.68	38.79
	39.19	40.75
Al_xFe	29.12	26.36
	28.95	25.06

650°C, represents melting of the eutectic constituent. The second peak corresponds to liquidus temperature of the alloy (about 750°C). During cooling, the exothermic peak of the nucleation temperature was recorded. DTA results were summarized in Table I. These nucleation temperatures are plotted on the Murray's metastable phase diagram [15] of Fig. 4a. The emulsified powders were collected and cleaned for observation of cross-sectional microstructures using an optical microscope (OM) and a scanning electron microscope (SEM). Fig. 4b to e show the cross-sectional microstructures of droplets taken with an OM. Also SEM results are in Fig. 5. Figs 4b and 5a show the typical morphologies of the average diameter of 240 μm powders. The undercooling was 37 K and primary $Al_{13}Fe_4$ phases were presented. The EDS result of the primary phase shows the stoichiometry range 35–41wt%Fe (Table II). These particles often exhibit a blade [5] or lath shape with the longest dimension between 50 and 120 μm. $Al_{13}Fe_4$ phase is an analogy to a stable phase of Al_3Fe. The matrix was a stable irregular Al-Al_3Fe eutectic phase. The 140 μm powders are shown in Figs 4c and 5b. A star-like primary $Al_{13}Fe_4$ phase was mainly formed ($\Delta T = 85$ K). The shape of the primary $Al_{13}Fe_4$ phase changes from lath-type to star-like as ΔT increases from 37 K to 85 K. Fig. 5b shows the typical morphology of primary ten-point stars of $Al_{13}Fe_4$ [16]. The α-Al cellular and the metastable Al-Al_6Fe eutectic were also presented in the matrix. It means that the matrix morphology of the eutectic changes from stable irregular Al-Al_3Fe to metastable regular Al-Al_6Fe between $\Delta T = 37$ K and $\Delta T = 85$ K. Al_3Fe phase increases the branching with an increasing growth rate [17]. Figs 4d and 5c show the microstructure of 63 μm powders with $\Delta T = 140$ K. The primary $Al_{13}Fe_4$ phase disappeared and the metastable primary Al_xFe phase dominated. The typical EDS result of the primary Al_xFe phases shows the stoichiometry range 25–29wt%Fe (Table II). These primary particles display a blocky shape with the longest dimension between 20 and 47 μm. Also the α-Al cellular and metastable regular Al-Al_6Fe eutectic were presented in the matrix. Young and Clyne observed the transition from $Al_{13}Fe_4$ to Al_xFe phases with an increasing cooling rate [7]. Based on the present

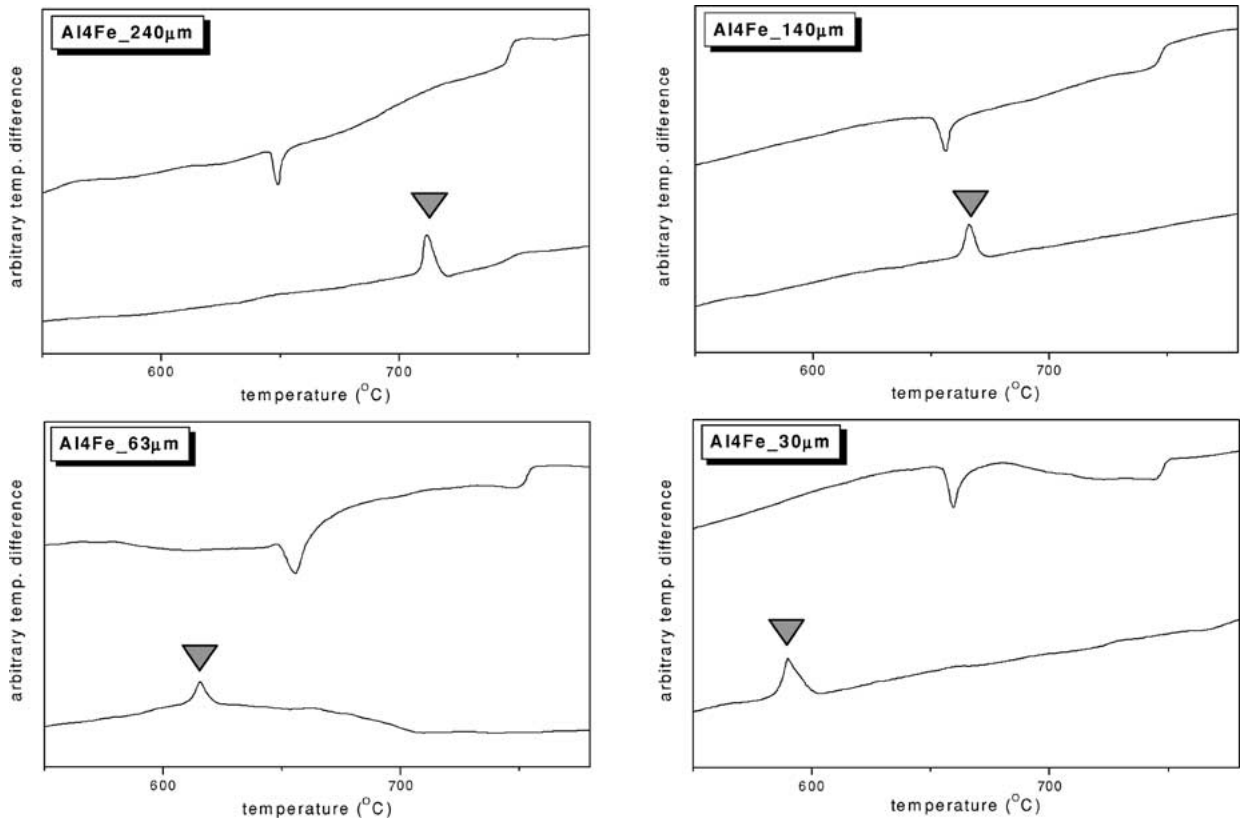

Figure 3 DTA thermograms of Al-4Fe powders.

results, the change of the primary phase occurs between $\Delta T = 85$ K and $\Delta T = 140$ K. The powders of the average diameter of 30 μm and $\Delta T = 160$ K are shown in Figs 4e and 5d. There are no primary phases, for example $Al_{13}Fe_4$ or Al_xFe, but only the eutectic of α-Al cellular and Al-Al_6Fe was shown. Fig. 6 summarizes the microstructural sequence of the primary phase and the eutectic by undercooling.

4. Discussion

The formation of various phases is influenced by the degree of undercooling experienced by the powders. The solid/liquid interface growth velocity of a particular phase can be related to the amount of undercooling of the powders prior to solidification [18]. Gilgien *et al.* [13] summarized the relationship between the composition, interface growth rate and microstructure formation for Al-Fe alloys using a microstructure selection map (MSM). They made the experiments on the Al-Fe alloys under temperature gradient $G > 0$ condition, using Bridgman solidification and laser melting, whose solidification microstructures were controlled mainly by the growth behaviors. In the present study, however, Al-Fe alloy powders that were manufactured by DET might be solidified in $G < 0$ condition and both nucleation as well as growth behaviors occurred. The undercooling, measured quantitatively, therefore causes both nucleation and growth behaviors. In the Al-4wt%Fe, using previous data [13] the undercooling could be calculated from the relationship between solidification velocity and undercooling. For solidification conditions in the Al-Fe system, Chu *et al.* [19] derived kinetic relationships based on LKT theory [20] between interface growth velocity V and undercooling ΔT. For Al-4Fe alloy powders, the relationships were approximately expressed as

$$V = 8.85 \times 10^{-6} \Delta T^{\alpha}$$

where

$$\alpha = 3.66 - 0.36 \log \Delta T$$

for V and ΔT in m/s and K, respectively. Table III shows a comparison of undercooling between calculated and experimental data. The microstructure variations due to the undercooling were used to build a MSM for an Al-Fe system (Fig. 7). The previous results were also superimposed to be compared.

As shown in Table III and Fig. 7, there are considerable differences between experimental undercooling and previous data based on LKT theory. That is, the amounts of undercooling of the previous report are much smaller than those of the present. The main reason for the differences may result from the solidification process differences between the two experiments. In the present experiment, both the nucleation and growth

TABLE III Comparison of the amount of undercooling (in K) between Gilgien *et al.* [13] and experimental data for Al-4Fe alloy powders

Phases	Al_3Fe + eut.Al-Al_3Fe	Al_3Fe + eut.Al-Al_6Fe	Eut. Al-Al_6Fe	Al_xFe + eut.Al-Al_6Fe	Al + eut.Al-Al_6Fe	Banded structure
Gilgien *et al.*	2	4	7	–	34	79
Experimental	37	85	–	140	160	–

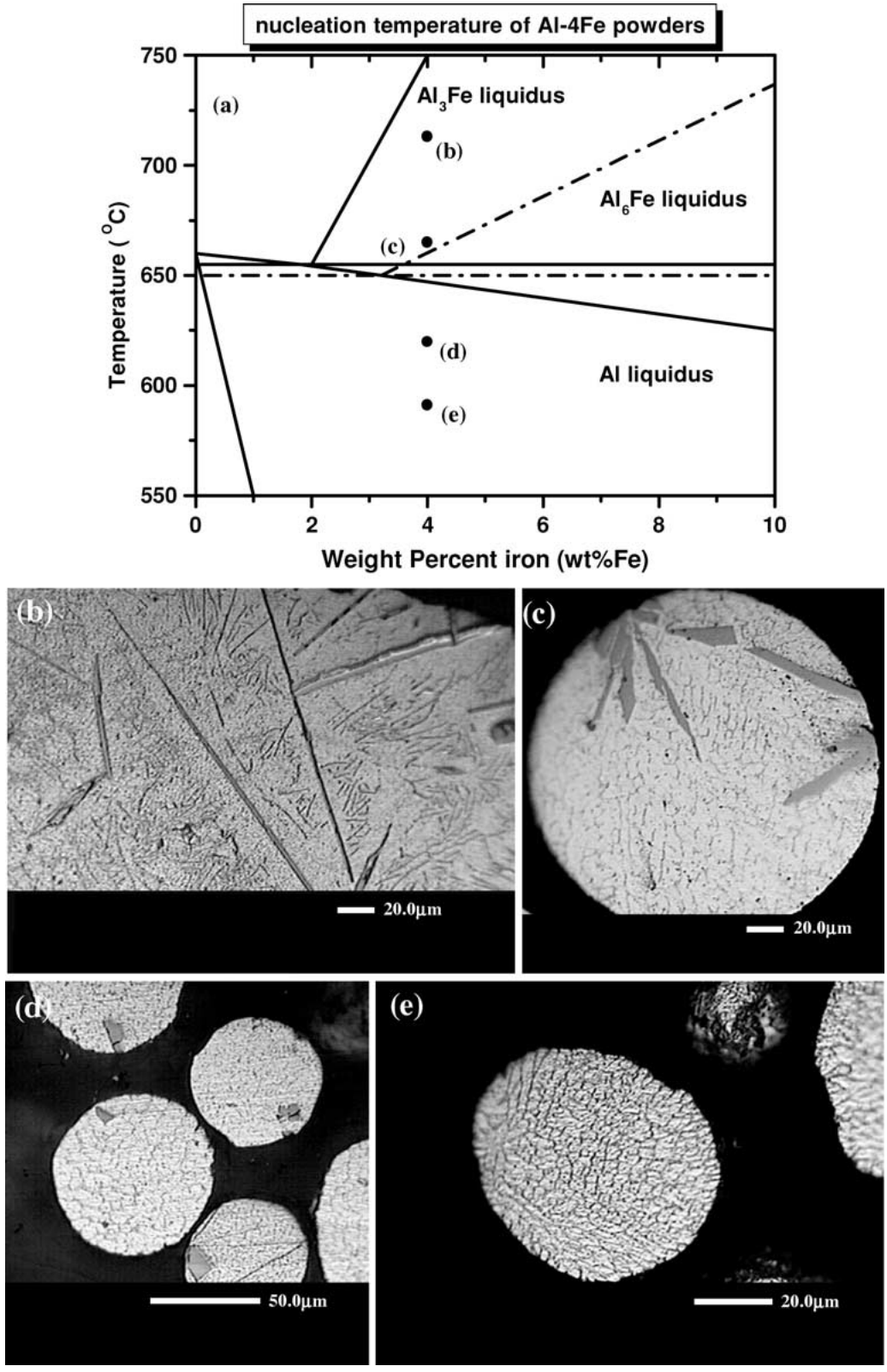

Figure 4 Size dependence of nucleation temperature for Al-4Fe alloy droplet and cross-sectional microstructure (OM) of droplets.

occur in the solidification, while only the growth occurs in the previous solidification researches. Therefore, the amount of the undercooling may represent different processes. The recalescence occurs due to the liberated heat of fusion when a part of the undercooled droplet solidified on the adiabatic condition [21]. The temperature of the remaining liquid phase increases up to the melting point by recalescence and the rest of the droplet solidified completely. For example, in the present powder solidification process, though the initial undercooling before solidification was large, most of that was consumed at the nucleation stage, therefore, only a small amount of the undercooling could be used for growth. Since the final microstructures usually depended on the growth behavior, the amount of undercooling which was detected on DTA did not agree with the process, in which only growth determined the microstructures.

The microstructures corresponding to the experimental undercooling can also be changed by coarsening or

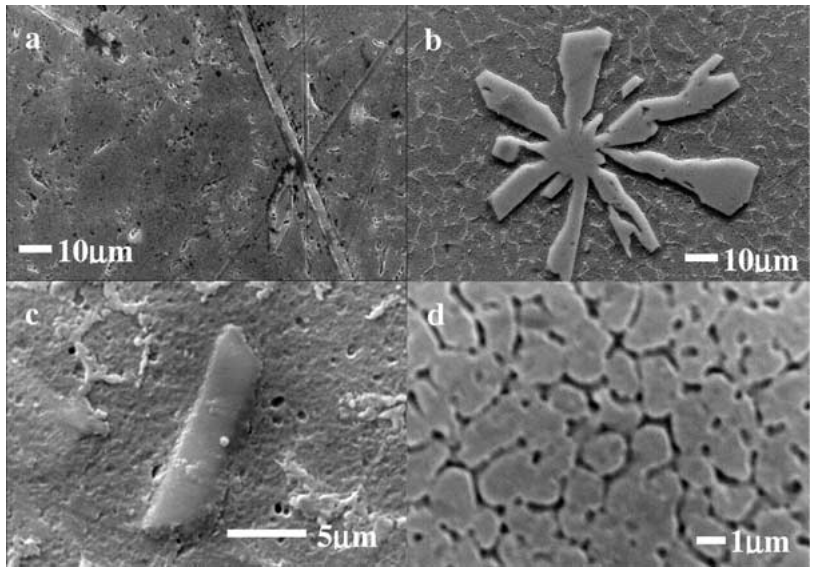

Figure 5 The cross-sectional microstructure (SEM) of Al-4Fe alloy powders at (a) 240 μm (b) 140 μm (c) 63 μm (d) 30 μm respectively.

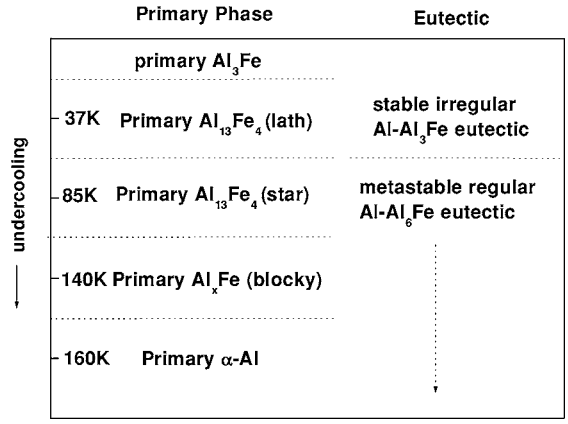

Figure 6 The microstructural sequences of the primary phase and the eutectic by the undercooling.

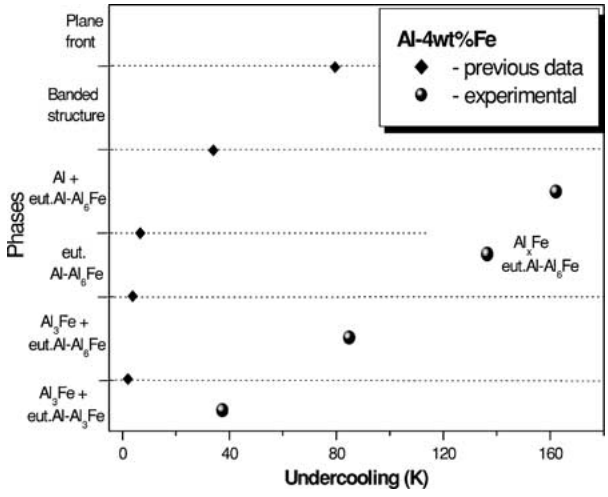

Figure 7 Microstructure selection map of Al-4wt%Fe alloy ($G < 0$).

decomposition. Coarsening influences the matrix, however the shape and composition of primary phases are not changed. Microstructural transition by decomposition hardly occurs in this study because the microstructural observation was performed at room temperature.

As shown in Fig. 4a, according to Murray's metastable phase diagram, to nucleate the Al_6Fe phase in the Al-4wt%Fe system, the solidification should be depressed at least under the metastable liquidus of the Al_6Fe phase. Also, more than 100 K undercooling needed to form the α-Al phase. However, the amount of undercooling converted from the LKT theory in the growth experiments was only a few degrees. Therefore, the present results agree well with Murray's phase diagram and explained well the behaviors of the solidification process having both nucleation and growth stage in it.

However a fully eutectic Al-Al_6Fe phase was not presented in emulsified powders. Instead of this phase, primary Al_xFe and eutectic Al-Al_6Fe phases were presented. Also, banded structure and plane front were not presented. If higher undercooling, and $\Delta T > 162$ K are achieved, banded structure and plane front phases can be acquired.

5. Conclusions

In the present study, Al-4Fe powders were prepared by DET. The undercooling was achieved at about 37 K–160 K by decreasing the powder size. The emulsified Al-4wt%Fe alloy powders showed several different microstructures depending on the amount of undercooling prior to solidification such as the $Al_{13}Fe_4$, Al_xFe phase, Al-Al_3Fe eutectic, Al-Al_6Fe eutectic and α-Al cellular structure. The shape of primary $Al_{13}Fe_4$ phase changes from lath-type to star-like as ΔT increases from $\Delta T = 35$ K to $\Delta T = 85$ K. The α-Al cellular and Al-Al_6Fe eutectic were also presented in the matrix. It means that matrix morphology of eutectic changes from irregular Al-Al_3Fe to metastable regular Al-Al_6Fe between $\Delta T = 37$ K and $\Delta T = 85$ K. The transition from $Al_{13}Fe_4$ to Al_xFe phases occurs between $\Delta T = 85$ K and $\Delta T = 140$ K. The powders of the average diameter of 30 μm and $\Delta T = 160$ K shows only the eutectics of α-Al cellular and metastable regular Al-Al_6Fe with no primary phases, for example $Al_{13}Fe_4$ and Al_xFe. Undercooling of previous data based on LKT theory is compared with experimental undercooling. Therefore the particular phases demonstrated using a MSM under the $G < 0$ condition. The present results can be

utilized as the fundamentals of the "tailored solidification" caused the microstructural transitions according to the solidification conditions.

Acknowledgements

The support of the Korea Science and Engineering Foundation (R01-2001-000-00258-0) for research is gratefully acknowledged.

References

1. J. D. COTTON and M. J. KAUFMAN, *Met. Trans.* A. **22A** (1991) 927.
2. R. F. COCHRANE, P. V. EVANS and A. L. GREER, *Mat. Sci. & Eng.* A **l33** (1991) 803.
3. H. JONES, *Mat. Sci. Eng.* **5** (1969/1970) 1.
4. M. G. CHU and D. A. GRANGER, *Met. Trans.* A **21A** (1990) 205.
5. W. J. BOETTINGER, L. BENDERSKY and J. G. EARLY, *ibid.* **17A** (1986) 781.
6. X. P. NIU, L. FROYEN, L. DELAEY and C. PEYTOUR, *J. Mater. Sci.* **29** (1994) 3724.
7. R. M. K. YOUNG and T. W. CLYNE, *Scripta Metall.* **15** (1981) 1211.
8. P. SKJERPE, *Met. Trans.* A **13** (1986) 189.
9. H. WESTENGEN, *Z. Metallkde* **73** (1982) 360.
10. A. M. B. DOUGLAS, *Acta Crystallogr.* **3** (1950) 19.
11. C. J. SIMENSEN and R. VELLASAMY, *Z. Metallk.* **68** (1977) 428.
12. P. SKJERPE, *Acta Crystallogr.* **44B** (1988) 486.
13. P. GILGIEN, A. ZRYD and W. KURZ, *Acta Metall.* **43** (1995) 3477.
14. J. H. PEREPEZKO, *Mat. Sci. Eng.* **65** (1984) 1548.
15. J. L. MURRAY, *Mat. Res. Soc. Symp. Proc.* **19** (1983) 249.
16. E. LOUIS, R. MORA and J. PASTOR, *Metal Sci. Dec.* (1980) 591.
17. C. McL. ADAM and L. M. HOGAN, *Acta Metall.* **23** (1975) 345.
18. J. A. JUAREZ-ISLAS, Y. ZHOU and E. J. LAVERNIA, *J. Mater. Sci.* **34** (1999) 1211.
19. M. G. CHU and D. A. GRANGER, *Met. Trans.* A **21A** (1990) 205.
20. J. LIPTON, W. KURZ and R. TRIVEDI, *Acta Metall.* **35** (1987) 957.
21. J. S. KIM and W. Y. YOON, *J. Korean Inst. Met. & Mater.* **31** (1993) 801.

Received 26 April 2001
and accepted 12 June 2002